Desalination and Water Treatment
www.deswater.com
doi: 10.1080/19443994.2015.1040849

57 (2016) 10646–10654
May

Taylor & Francis
Taylor & Francis Group

Zirconium-immobilized bentonite for the removal of methyl orange (MO) from aqueous solutions

Ruihua Huang[a,*], Chen Hu[a], Bingchao Yang[b], Jing Zhao[a]

[a]*College of Science, Northwest A&F University, Yangling, Shaanxi 712100, China, emails: hrh20022002@163.com (R. Huang), 931794700@qq.com (C. Hu), 723152125@qq.com (J. Zhao)*
[b]*Xi'an Institute of Geology and Mineral Resource, Xi'an, Shaanxi 710054, China, email: 87413199@qq.com*

Received 3 July 2014; Accepted 27 March 2015

ABSTRACT

Zirconium-immobilized bentonite was prepared by hydrothermal reaction, and characterized by scanning electronic microscope (SEM) and X-ray diffraction (XRD) techniques. Removal of methyl orange (MO) from aqueous solutions with zirconium-immobilized bentonite was investigated by a batch method. These factors including adsorbent dosage, pH value of MO solution, and contact time were evaluated. Adsorption equilibrium was achieved at 60 min or so. The experimental isotherm data were described by the Langmuir isotherm model. The maximum adsorption capacity obtained from the Langmuir isotherm model was 44.13 mg/g at 298 K and natural pH value. An increase in temperature reduced the adsorption of MO while the increasing amount of zirconium enhanced the adsorption of MO onto Zr-immobilized bentonite. 1 M HCl was identified as the best eluent.

Keywords: Methyl orange; Adsorption; Zirconium-immobilized bentonite; Isotherm

1. Introduction

With the rapid development of modern industries, water pollution is getting worse. Dyes have become one of the main sources of water pollution. The release of the effluent-containing dyes has triggered a major concern on the human health as well as marine lives. Therefore, various methods including chemical precipitation, coagulation and flocculation, ion exchange, membrane filtration, biological treatment, and adsorption have been employed for the removal of these pollutants from wastewaters [1–4]. Among these methods, adsorption has been considered as an effective method due to its simplicity of design, ease of operation, and high efficiency [5].

A large variety of adsorbent materials have been studied to remove dyes from aqueous solutions, such as activated carbon, chitosan, cellulose, and bentonite. Bentonite, as an effective adsorbent, has received much attention recently and been widely used for the removal of dyes from wastewaters due to its low cost and its abundance in various parts of the world [6–8]. However, the original bentonite showed low adsorption capacity for anion dyes due to the negatively charged and hydrophilic particle surfaces [9]. Some physical and chemical methods were applied for the modification of bentonite to improve its adsorption capacity toward anion dyes.

As we known, the high negative charge of bentonite surfaces is usually balanced by metals cations. These cations can be replaced by inorganic hydroxyl-metal polycations acting as pillars which increase the

*Corresponding author.

interlayer spacing of bentonite. Pillared bentonites were often obtained by three-step method including the preparation of pillars, the intercalation of pillars in bentonite, and the calcination process [10–12]. Various inorganic-pillared bentonites have been prepared and employed to remove heavy metals [13], dyes [14–16], and other environmental pollutants [17,18]. Among these pillars, poly-hydroxyl zirconium is one of the most used pillars [19], whose structure is $[Zr_4(OH)_{14}(H_2O)_{10}]^{2+}$. The Zr-pillared clay usually has a large basal spacing and microporous structure, and shows better thermal stability and performance of adsorption for organic compounds and metals as compared with Al-pillared clay [20].

In this study, zirconium-immobilized bentonite was prepared by two-step method including calcination and hydrothermal reaction. The resultant bentonite was characterized by scanning electronic microscope (SEM) and X-ray diffraction (XRD) techniques, and its adsorption capacity for methyl orange (MO) was studied. Parameters affecting the adsorption of MO such as the ratio of Zr to bentonite, adsorbent dosage, pH, contact time, and initial MO concentration were investigated, and the adsorption isotherms were also studied. In addition, the regeneration of zirconium-immobilized bentonite was evaluated.

2. Materials and methods

2.1. Materials

Bentonite powder with a particle size of 200 mesh was acquired from the chemical factory of Shentai, Xinyang, Henan, China. MO was supplied by Sigma chemical company, and used as adsorbate in the tests. MO concentrations were measured using a UV–vis spectrometer at a wavelength of 464 nm. All other reagents used in this study were of analytical grade.

2.2. Preparation of zirconium-immobilized bentonite

Firstly, the original bentonite was calcined for 2 h at 773 K. Calcined bentonite and zirconium oxychloride solution ($ZrOCl_2{\cdot}8H_2O$) were added to 30 ml of distilled water, and the ratio of zirconium to bentonite was 1.2 mmol/g. The suspension was placed in a tightly capped 50 mL Teflon-lined stainless steel reactor. The reactor was kept in an oven under static condition at 393 K for 12 h. After the hydrothermal reaction was performed, the samples were filtered and washed with distilled water several times, and dried in an oven at 333 K for 12 h. After drying, it was ground and sieved. Zirconium-immobilized bentonite composite with 200 mesh of particle size was collected and utilized for batch experiments.

2.3. Characterization of zirconium-immobilized bentonite

In order to confirm the crystal structure and mineralogy of zirconium-immobilized bentontie, XRD was performed by a Shimadzu XD3A diffractometer equipped with a monochromatic Cu Ka source operating at 40 kV and 30 mA. The diffraction patterns were recorded from 3° to 55° with a scan rate of 0.02°/s. The structure and morphology of bentonite samples were determined by field emission scanning electronic microscope (FE-SEM) (Hitachi S4800). Besides, the pH value at point zero charge (pH_{pzc}) of zirconium-immobilized bentonite was determined by the solid addition method.

2.4. MO adsorption experiment

Adsorption of MO was carried out by the batch method. The effects of adsorbent dosage, initial pH value of dye solution, and contact time were investigated. The adsorption experiments were performed by a batch method in stopper conical flasks containing 50 mL of MO solutions with various concentrations and the given dosage of adsorbent. These samples were agitated on a thermostated shaker at 200 rpm at 298–323 K. pH value of dye solutions was adjusted with 0.1 M HCl or NaOH solutions. When the defined time attained, the supernatant was filtered through filter paper to determine the residual concentrations.

The initial and final MO concentrations were analyzed using a UV spectrophotometer. The removal (R, %) and the amounts of MO adsorbed at time t (q_t, mg/g) and at equilibrium (q_e, mg/g) were calculated using the following equations:

$$R = 100 \times \frac{(C_0 - C_t)}{C_0} \tag{1}$$

$$q_e = (C_0 - C_e) \times \left(\frac{V}{M}\right) \tag{2}$$

$$q_t = (C_0 - C_t) \times \left(\frac{V}{M}\right) \tag{3}$$

where C_0, C_t, and C_e (mg/L) are the initial, time t, and equilibrium concentrations of MO solution, respectively; V (L) is the volume of MO solution; and M (g) is the weight of absorbent.

2.5. Desorption experiment

Desorption studies will help to regenerate the zirconium-immobilized bentonite, so that it can be reused to adsorb MO. All the regeneration experiments were carried out at room temperature. After performing the equilibrium study with initial MO concentration of 300 mg/L, MO-adsorbed particles were collected by filtration, and eluted with different HCl concentrations ranging from 0.05 to 3 mol/L. The particles were removed and rinsed with distilled water and then reused for the adsorption of MO solutions.

3. Results and discussion

3.1. SEM and XRD analyses

SEM was used to study the morphological features of bentonite, calcined bentonite, zirconium-immobilized bentonite, and zirconium-immobilized bentonite loaded by MO. The surface morphology of bentonite was different from that of calcined bentonite and zirconium-immobilized bentonite (Fig. 1). The original bentonite before calcination appeared as cornflake-like crystals, revealing the extremely fine platy structure. For calcined bentonite, this platy structure was destroyed to some degree, and the clay became porous and fluffy. After the calcined bentonite was immobilized by zirconium, the clay had become more porous and fluffy. The existence of this porous and fluffy structure can be attributed to the cation exchanges and the reduction in certain amorphous phase within calcined bentonite [21]. However, zirconium-immobilized bentonite loaded by MO presented a relatively compact structure due to the cluster of MO onto the clay surface as compared with zirconium-immobilized bentonite.

XRD patterns of bentonite, calcined bentonite, zirconium-immobilized bentonite, and MO adsorbed zirconium-immobilized bentonite are shown in Fig. 2. XRD pattern of bentonite showed a typical reflection of montmorillonite in bentonite at $2\theta = 6.56^{\circ}$. In calcined bentonite, this peak shifted to $2\theta = 8.78^{\circ}$, suggesting that the interlayer spacing decreased. A similar result was also reported by Vieira et al. [22]. This decrease may be attributed to the fluffy structure of bentonite and the release of a part of interlayer impurities in bentonite due to calcination. Meanwhile, a decrease in the intensity of this peak was observed. A decrease in the intensity may be due to a slight distortion of the intrinsic lattice arrangement of the silicate layers, and a decrease in the crystallinity caused by calcination. In zirconium-immobilized bentonite, the peak of montmorillonite shifted from $2\theta = 8.78^{\circ}$ to $2\theta = 5.63^{\circ}$, indicating an increase in the interlayer spacing, which can be attributed to the expansion of the clay layer during hydrothermal reaction. This proved that the bigger Zr oligomer may be located in the interlayer space of bentonite layer and caused structural changes. Further, it was found that the XRD pattern of zirconium-immobilized bentonite after MO adsorption had no changes as compared with the one of zirconium-immobilized bentonites, suggesting that MO was only adsorbed on the inside and outside surfaces of adsorbent.

3.2. Determination of pH_{pzc} of zirconium-immobilized bentonite

The effect of pH on adsorption can be described on the basis of point zero charge (pH_{pzc}), which is the point at which the net charge of the adsorbent is zero [23]. The pH_{pzc} of the adsorbent was determined by the solid addition method [24]. Initial pH of 0.1 mol/L NaCl solutions (pH_i) was adjusted from pH 1 to 11 by adding either 0.1 mol/L HCl or 0.1 mol/L NaOH. Adsorbent dose (0.4 g) was added to 50 mL of 0.1 mol/L NaCl solution in 150 mL conical flasks and stirred for 60 min and final pH (pH_f) of solution was measured. The difference between the initial and final pH ($pH_f - pH_i$) was plotted against the initial pH (pH_i) and the point where $pH_f - pH_i = 0$ was taken as the pH_{pzc} (Fig. 3). The pH_{pzc} of zirconium-immobilized bentonite was found to be 2.2.

3.3. Effect of adsorbent dosage on MO adsorption

In order to investigate the effect of adsorbent dosage, various amounts of zirconium-immobilized bentonite were added to 50 mL MO solutions (100 and 200 mg/L) at 298 K. As shown in Fig. 4, the removal increased from 36.8 to 96.6% and from 30.6 to 90.7%, respectively, with an increase in adsorbent dosage from 0.1 to 0.4 g. This increase can be ascribed to the increasing sites available for MO adsorption. However, the removal increased slowly when the dosage was beyond 0.4 g. This may be attributed to the attainment of equilibrium between the adsorbate and the adsorbent under the operating conditions. In this study, 0.4 g of adsorbent dosage was adopted for further experiments because the removal of MO solutions tested was more than 90%.

3.4. Effect of pH on MO adsorption

The pH of the aqueous solution is an important controlling parameter in adsorption. The effect of pH on the adsorption of MO onto zirconium-immobilized bentonite was studied in the range of 3–11. The

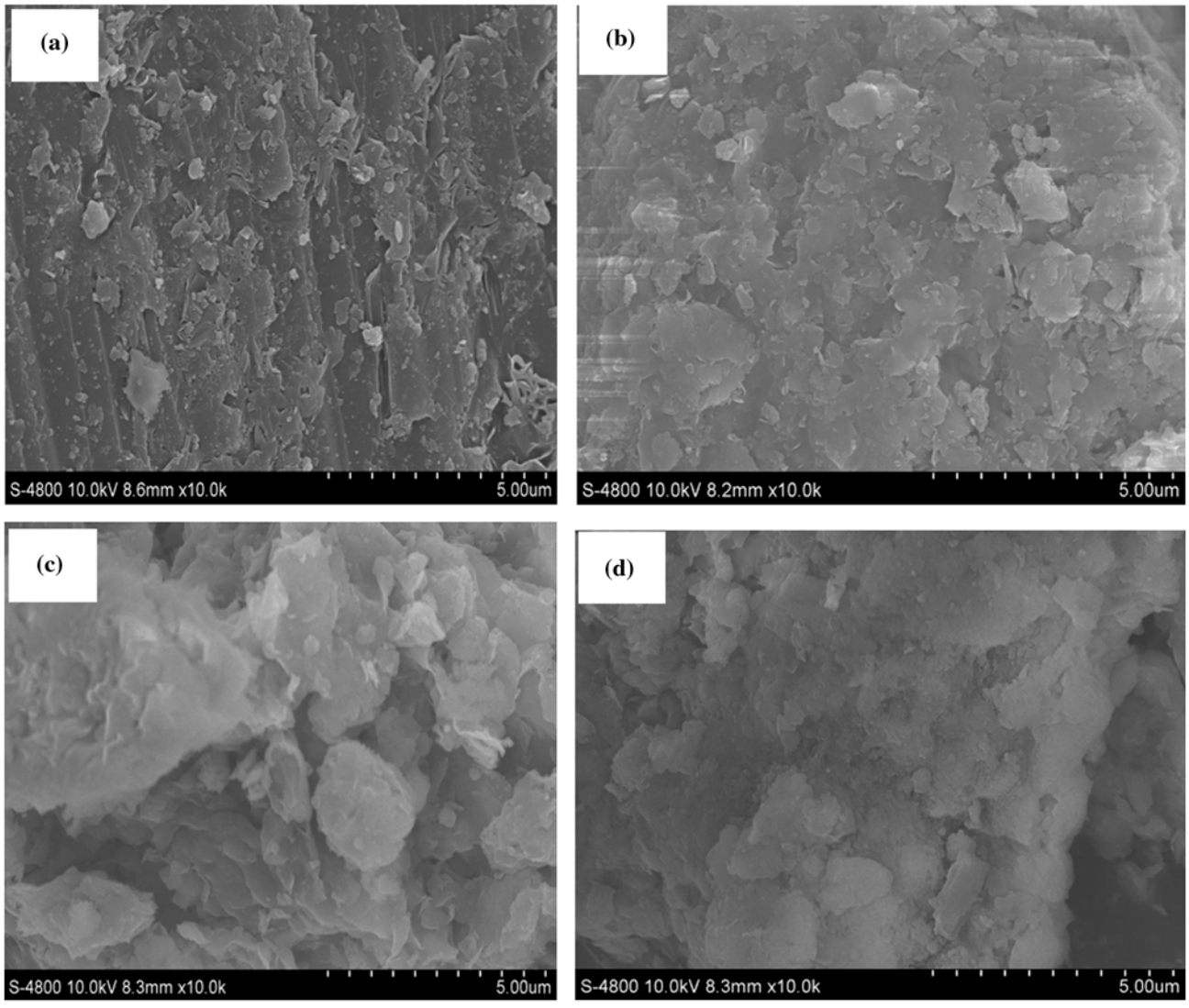

Fig. 1. SEM images of bentonite (a), calcined bentonite (b), zirconium-immobilized bentonite (c), and zirconium-immobilized bentonite loaded by MO (d).

experiments were carried out at 298 K with 50 mL MO solutions (100 and 200 mg/L) at a fixed dosage of 0.4 g. The results are shown in Fig. 5. The removal decreased gradually with the increasing pH from 3 to 8. A drastic decrease was observed when the pH value exceeded 8.0. MO has two chemical structures, whose chromophores are anthraquinone or azo bond depending on the pH of the solution [25], as can be expressed as follows:

The pK_a value of MO in water is close to 3.4 [26]. The sulfonate groups of MO dyes (–SO_3Na) were dissociated and converted to anionic dye ions –SO_3− in aqueous solution at all over the pH range studied. The surface chemistry of the adsorbents is an important factor that controls the adsorption of adsorbate. Adsorbent has a net negative charge on its surface when the pH value of the solution is higher than its pH_{pzc}, whereas it has a net positive charge when the

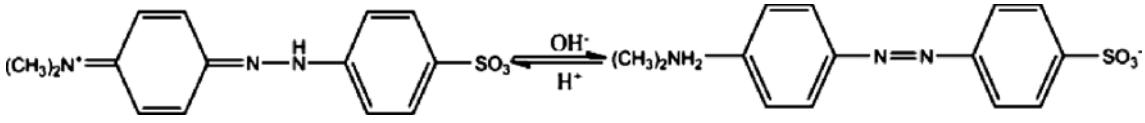

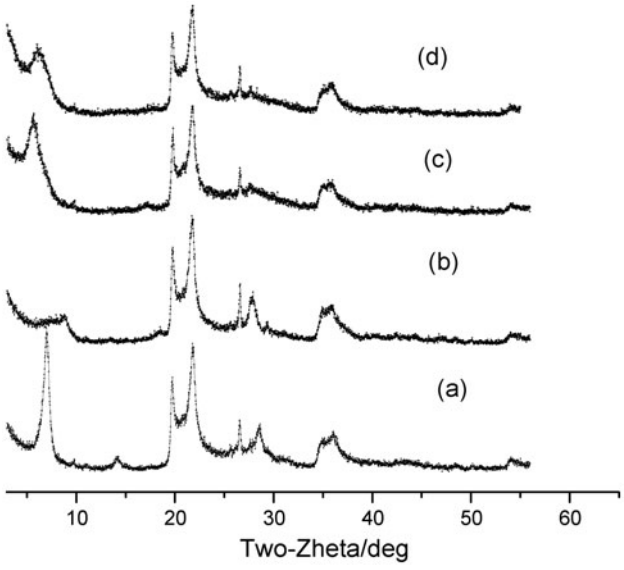

Fig. 2. XRD patterns of bentonite (a), calcined bentonite (b), zirconium-immobilized bentonite (c), and MO adsorbed zirconium-immobilized bentonite (d).

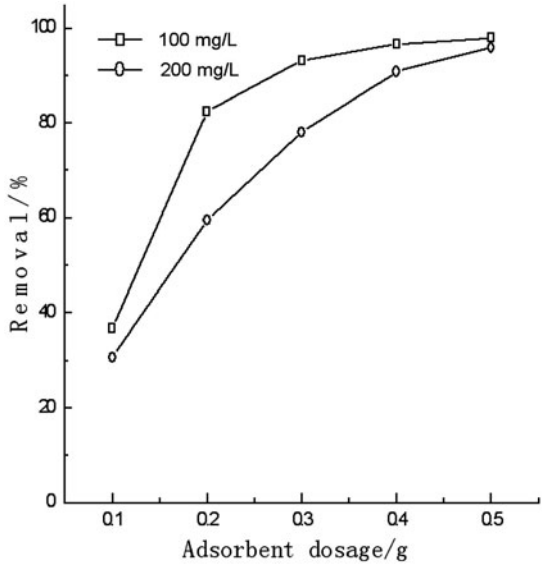

Fig. 4. Effect of adsorbent dosage on MO adsorption (initial dye concentrations: 100 and 200 mg/L; natural pH; temperature: 298 K; and contact time: 60 min).

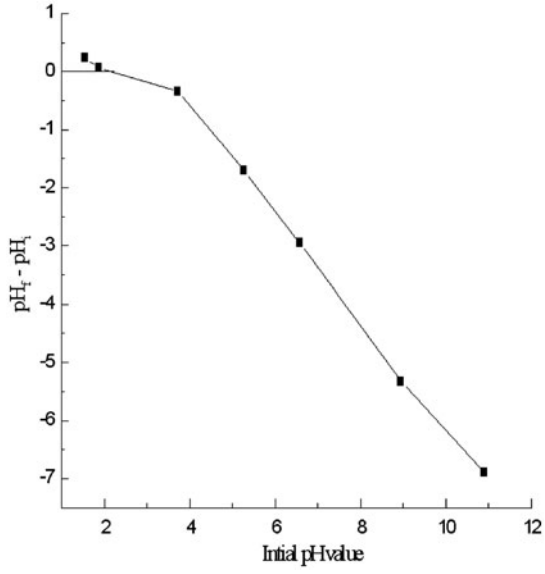

Fig. 3. Plot of $pH_f - pH_i$ vs. pH (adsorbent dose: 0.4 g; temperature: 298 K; and contact time: 60 min).

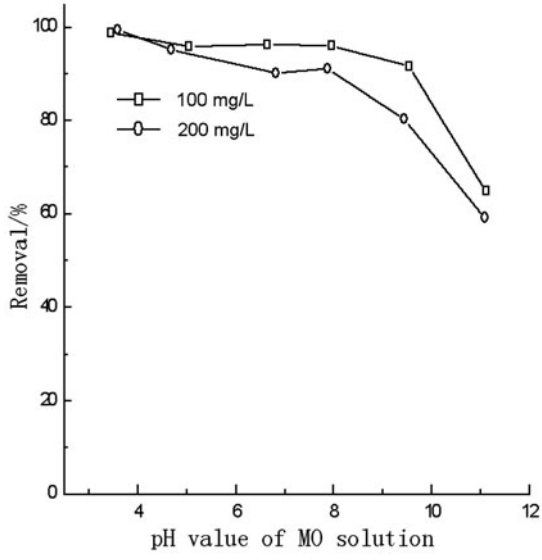

Fig. 5. Effect of pH values on MO adsorption (initial dye concentrations: 100 and 200 mg/L; adsorbent dose: 0.4 g; temperature: 298 K; and contact time: 60 min).

pH in the solution is lower than its pH_{pzc} [16]. As shown the results in Section 3.2, this zirconium-immobilized bentonite had a negative charge as the pH values tested were higher than its pH_{pzc} value (2.2), thus meaning that the electrostatic repulsion existed between the negatively charge surface and the negatively charged dye molecules. This repulsion was unfavorable for MO adsorption, resulting to decreasing removal. However, the porous and fluffy structure of zirconium-immobilized bentonite (see in Fig. 1) and the big interlayer spacing (see in Fig. 2) would facilitate the adsorption of MO onto zirconium-immobilized bentonite. Though increasing pH values weakened MO adsorption to some degree, this adsorbent showed high removal due to its specific structure

in the pH value range from 3 to 8. At a lower pH value, the MO existed in left pattern, the number of negatively charged sites in MO decreased, creating a decreasing repulsion between zirconium-immobilized bentonite and MO. As a result, there was a slight increase in the removal of MO from the solution. At higher pH values, low removal may be ascribed to the competition of abundant OH^- ions with anionic ions of MO for the adsorption sites. As the initial pH value of MO solution was near 6.8, and the adsorbent allowed relatively high removal at this pH value, the pH value of MO solution was not adjusted in the following experiments.

3.5. Effect of contact time and initial concentration

Fig. 6 showed the removal of MO by zirconium-immobilized bentonite with MO solutions (100, 200, 300, and 500 mg/L) at natural pH and 298 K. The adsorption rate increased quickly at the initial stage, and the adsorption equilibrium was reached after approximately 60 min. This trend may be ascribed to more adsorption vacant sites on zirconium-immobilized bentonite available for adsorption at the initial adsorption, and the existence of high concentration gradient of MO between the aqueous and solid phases. Subsequently, the concentration gradient from the solution to the solid was reduced due to the fact that most of the vacant sites were occupied by dye molecules, resulting in a slightly decrease in adsorption during the later stages [27]. Meanwhile, it can be observed from Fig. 6 that the removal of MO decreased from 96.5 to 57.2% with increasing the initial concentration of MO from 100 to 500 mg/L. This effect could be explained as follows. At low MO concentrations, the adsorbent/adsorbate ratios were big, and thus the available site were enough for the adsorption of MO, leading to high removal. However, as MO concentration increased, the adsorbent/adsorbate ratios decreased and fewer sites were used for adsorption, and so the removal reduced.

3.6. Adsorption isotherms

In order to describe the adsorption process of MO onto zirconium-immobilized bentonite, two adsorption isotherms were used to evaluate the experimental results. Langmuir isotherm is applicable under the following hypothesis: the adsorbent has a uniform surface; the absence of interactions between the adsorbent molecules; and the adsorption process takes place in a single layer. The linear form of the Langmuir equation is given in Eq. (4):

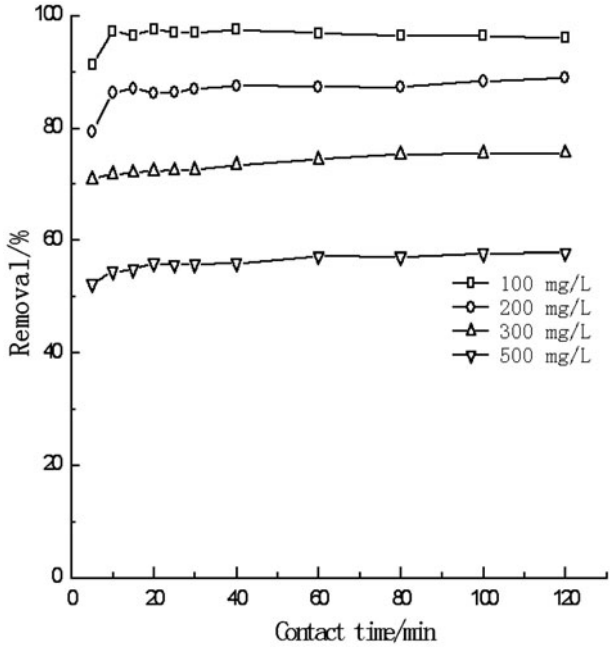

Fig. 6. Effect of contact time and MO concentrations on MO adsorption (initial dye concentrations: 100, 200, 300, and 500 mg/L; natural pH; adsorbent dose: 0.4 g; and temperature: 298 K).

$$\frac{C_e}{q_e} = \frac{1}{Q_b} + \frac{C_e}{Q} \tag{4}$$

where q_e (mg/g) is the equilibrium amount of MO adsorption by zirconium-immobilized bentonite, C_e (mg/L) is the equilibrium MO concentration in the solution, Q (mg/g) is the maximum adsorption of MO, and b (L/mg) is the Langmuir constant related to the enthalpy of the process. b and Q are the constants that can be calculated from the intercept and slope of the linear plot between C_e/q_e and C_e.

The Freundlich isotherm describes heterogeneous systems, i.e. compounds with adsorbent surfaces and non-energetically equivalent binding sites. The linear form of Freundlich isotherm is described according to the following Eq. (5):

$$\log q_e = \log K_f + \frac{1}{n}\log C_e \tag{5}$$

K_f ((mg/g)(L/mg)$^{1/n}$) and $1/n$ are the Freundlich constants related to adsorption capacity and heterogeneity factor, respectively. The higher value for K_f indicates higher affinity for adsorbate and the value of the empirical parameter $1/n$ lies between $0.1 < 1/n < 1$, indicating favorable adsorption. K_f and $1/n$ can be determined from the linear plot of log q_e vs. log Ce.

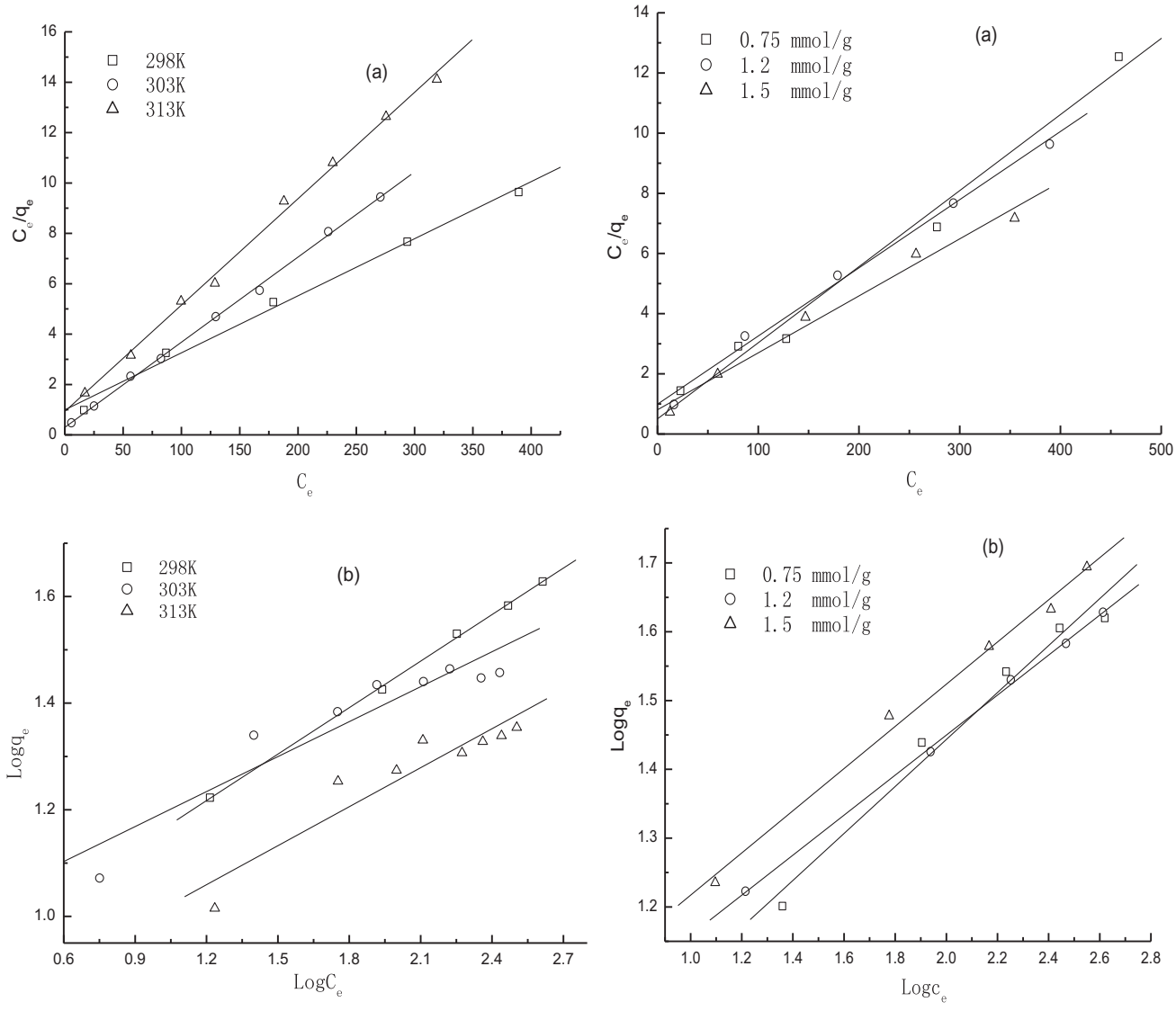

Fig. 7. Langmuir (a) and Freundlich (b) isotherm models of MO adsorption onto zirconium-immobilized bentonite.

The two isotherm models are illustrated in Fig. 7. Parameters and correlation coefficients obtained from the two isotherm models are summarized in Table 1. From Table 1, the Langmuir adsorption model was found to fit the experimental data for MO adsorption in accordance with the higher liner correlation coefficients. It indicates the homogeneity of active sites on the surface of zirconium-immobilized bentonite. Meanwhile, the values of Q decreased with increasing the temperature, indicating that the adsorption process was exothermic. The maximum of adsorption capacity reached 44.13 mg/g at 298 K according to the Langmuir model. The Freundlich values of $1/n$ obtained at all conditions tested were between 0 and 1, indicating that the adsorption of MO onto zirconium-immobilized bentonite was attributed to favorable adsorption.

3.7. Desorption studies

In this study, the adsorption was operated by adding 0.4 g of zirconium-immobilized bentonite in 50 mL 100 mg/L MO solution and shaking for 60 min at 298 K. In the desorption process, zirconium-immobilized bentonite samples loaded by MO were added into 50 mL of HCl solutions with different concentrations which were used as the eluent. After desorption, these samples were washed with distilled water several times, and dried, and it was applied for the adsorption

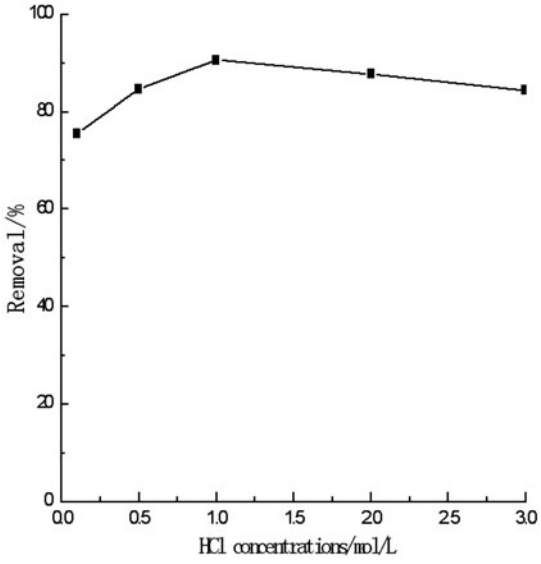

Fig. 8. Plot for the removal of MO with HCl eluent concentrations.

Table 1
Adsorption isotherm parameters of MO onto zirconium-immobilized bentonite

	Langmuir			Freundlich		
Parameters	K	Q	R^2	K_f	$1/n$	R^2
Temperature/K						
298 K	0.0228	44.13	0.9966	7.381	0.2908	0.9935
303 K	0.1126	29.59	0.9995	9.370	0.2186	0.9378
313 K	0.0456	23.67	0.9984	5.846	0.2438	0.9356
Ratio of Zr to bentonite						
0.75 mmol/g	0.0502	39.54	0.9924	5.762	0.3414	0.9872
1.2 mmol/g	0.0228	44.13	0.9966	7.381	0.2908	0.9935
1.5 mmol/g	0.0236	52.80	0.9929	8.318	0.3066	0.9904

of MO solution again. The values for the removal of MO for each eluent are presented in Fig. 8. Compared with the fresh adsorbent, the regenerated adsorbent with 1 mol/L HCl showed a slightly decrease in the removal of MO. Therefore, it is concluded that 1 mol/L HCl was identified as the best eluent.

4. Conclusions

In the present study, zirconium-immobilized bentonite was prepared by hydrothermal reaction, and its efficiency in removing MO was tested by batch adsorption technique. The SEM image of Zr-immobilized bentonite showed a porous and fluffy structure on the surface, which favored the adsorption of MO. XRD results confirmed the immobilization of Zr onto calcined bentonite. The removal increased when increasing the adsorbent dosage. The removal decreased with increasing MO concentrations. The equilibrium time was reached within 60 min. The adsorption isotherm data fit well to the Langmuir isotherm model and the maximum adsorption capacity of Zr-immobilized bentonite was 44.13 mg/g at 298 K and natural pH. This adsorbent loaded by MO was liable to be eluted with 1 mol/L HCl solution.

References

[1] Y.Y. Lau, Y.S. Wong, T.T. Teng, N. Morad, M. Rafatullah, S.A. Ong, Coagulation–flocculation of azo dye Acid Orange 7 with green refined laterite soil, Chem. Eng. J. 246 (2014) 383–390.
[2] Y. Haldorai, J.J. Shim, An efficient removal of methyl orange dye from aqueous solution by adsorption onto chitosan/MgO composite: A novel reusable adsorbent, Appl. Surf. Sci. 292 (2014) 447–453.
[3] F.M. Amaral, M.T. Kato, L. Florêncio, S. Gavazza, Color, organic matter and sulfate removal from textile effluents by anaerobic and aerobic processes, Bioresour. Technol. 163 (2014) 364–369.
[4] M. Auta, B.H. Hameed, Chitosan-clay composite as highly effective and low-cost adsorbent for batch and fixed-bed adsorption of methylene blue, Chem. Eng. J. 237 (2014) 352–361.
[5] S.K. Maji, Y.H. Kao, C.J. Wang, G.S. Lu, J.J. Wu, C.W. Liu, Fixed bed adsorption of As(III) on iron-oxide-coated natural rock (IOCNR) and application to real arsenic-bearing groundwater, Chem. Eng. J. 203 (2012) 285–293.
[6] Y.G. Chen, B.H. Zhu, D.B. Wu, Q.G. Wang, Y.H. Yang, W.M. Ye, J.F. Guo, Eu(III) adsorption using di(2-thylhexly) phosphoric acid-immobilized magnetic GMZ bentonite, Chem. Eng. J. 181–182 (2012) 387–396.
[7] D.B. Wu, C.M. Zhu, Y.G. Chen, B.H. Zhu, Y.H. Yang, Q.G. Wang, W.M. Ye, Preparation, characterization and adsorptive study of rare earth ions using magnetic GMZ bentonite, Appl. Clay. Sci. 62–63 (2012) 87–93.
[8] A.R. Nesic, S.J. Velickovic, D.G. Antonovic, Characterization of chitosan/montmorillonite membranes as adsorbents for Bezactive Orange V-3R dye, J. Hazard. Mater. 209–210 (2012) 256–263.
[9] A.S. Özcan, B. Erdem, A. Özcan, Adsorption of acid blue 193 from aqueous solutions onto Na-bentonite and DTMA-bentonite, J. Colloid. Interface Sci. 280 (2004) 44–54.
[10] S. Mnasri-Ghnimi, N. Frini-Srasra, Promoting effect of cerium on the characteristic and catalytic activity of Al, Zr, and Al–Zr pillared clay, Appl. Clay. Sci. 88-89 (2014) 214–220.
[11] D.M. Manohar, B.F. Noeline, T.S. Anirudhan, Adsorption performance of Al-pillared bentonite clay for the removal of cobalt(II) from aqueous phase, Appl. Clay. Sci. 31 (2006) 194–206.

[12] B.S. Mnasri, N. Frini-Srasra, Evolution of Brönsted and Lewis acidity of single and mixed pillared bentonite, Infrared Phys. Technol. 58 (2013) 15–20.
[13] J. Zhou, P. Wu, Z. Dang, N. Zhu, P. Li, J. Wu, X. Wang, Polymeric Fe/Zr pillared montmorillonite for the removal of Cr(VI) from aqueous solutions, Chem. Eng. J. 162 (2010) 1035–1044.
[14] P. Tepmatee, P. Siriphannon, Effect of preparation method on structure and adsorption capacity of aluminum pillared montmorillonite, Mater. Res. Bull. 48 (2013) 4856–4866.
[15] J.E. Aguiar, B.T.C. Bezerra, A.C.A. Siqueira, D. Barrera, K. Sapag, D.C.S. Azevedo, S.M.P. Lucena, I.J. Silva, Improvement in the adsorption of anionic and cationic dyes from aqueous solutions: A comparative study using aluminium pillared clays and activated carbon, Sep. Sci. Technol. 49 (2014) 741–751.
[16] A. Gil, F.C.C. Assis, S. Albeniz, S.A. Korili, Removal of dyes from wastewaters by adsorption on pillared clays, Chem. Eng. J. 168 (2011) 1032–1040.
[17] P.R. Pereira, J. Pires, M. Brotas de Carvalho, Adsorption of methane and ethane in zirconium oxide pillared clays, Sep. Purif. Technol. 21 (2001) 237–246.
[18] C.D. Bringle, I.G. Shibi, V.P. Vinod, T.S. Anirudhan, Sorption of humic acid from aqueous solutions by lanthana-alumina mixed oxide pillared bentonite, J. Sci. Ind. Res. 46 (2005) 782–788.
[19] M.R. Sun Kou, S. Mendioroz, M.I. Guijarro, A thermal study of Zr-pillared montmorillonite, Thermochim. Acta 323 (1998) 145–157.
[20] A. Gil, A. Massinon, P. Grange, Analysis and comparison of the microporosity in Al-, Zr-, Ti-pillared clays, Micropor. Mater. 4 (1995) 369–378.
[21] T.S. Anirudhan, C.D. Bringle, S. Rijith, Removal of uranium(VI) from aqueous solutions and nuclear industry effluents using humic acid-immobilized zirconium-pillared clay, J. Environ. Radioactiv. 101 (2010) 267–276.
[22] M.G.A. Vieira, A.F. Almeida Neto, M.L. Gimenes, M.G.C. da Silva, Sorption kinetics and equilibrium for the removal of nickel ions from aqueous phase on calcined Bofe bentonite clay, J. Hazard. Mater. 177 (2010) 362–371.
[23] E.N. El-Qada, S.J. Allen, G.M. Walker, Adsorption of methylene blue onto activated carbon produced from steam activated bituminous coal: A study of equilibrium adsorption isotherm, Chem. Eng. J. 124 (2006) 103–110.
[24] S.M. de Oliveira Brito, H.M.C. Andrade, L.F. Soares, R.P. de Azevedo, Brazil nut shells as a new biosorbent to remove methylene blue and indigo carmine from aqueous solutions, J. Hazard. Mater. 174 (2010) 84–92.
[25] S. Chen, J. Zhang, C. Zhang, Q. Yue, Y. Li, C. Li, Equilibrium and kinetic studies of methyl orange and methyl violet adsorption on activated carbon derived from *Phragmites australis*, Desalination 252 (2010) 149–156.
[26] L. Obeid, A. Bée, D. Talbot, J.S. Ben, V. Dupuis, S. Abramson, V. Cabuil, M. Welsch-billig, Chit- osan/-maghemite composite: A magsorbent for the adsorption of methyl orange, J. Colloid. Interface Sci. 410 (2013) 52–58.
[27] T.S. Anirudhan, C.D. Bringle, S. Rijith, Removal of uranium(VI) from aqueous solutions and nuclear industry effluents using humic acid-immobilized zirconium-pillared clay, J. Environ. Radioactiv. 101 (2010) 267–276.